Global Organization of Dynamics in Oscillatory Heterogeneous Excitable Media

Gil Bub,[1] Alvin Shrier,[2] and Leon Glass[2]

[1]*Department of Physiology and Pharmacology, State University of New York Downstate Medical Center, Brooklyn, New York 11203, USA*

[2]*Department of Physiology, McGill University, 3655 Promenade Sir William Osler, Montreal, Quebec, H3G 1Y6, Canada*

(Received 11 February 2004; published 20 January 2005)

An oscillatory heterogeneous excitable medium undergoes a transition from periodic target patterns to a bursting rhythm driven by the spontaneous initiation and termination of spiral waves as coupling or density is reduced. We illustrate these phenomena in monolayers of chick embryonic heart cells using calcium-sensitive fluorescent dyes. These results are modeled in a heterogeneous cellular automaton in which the neighborhood of interaction and cell density is modified. Parameters that give rise to bursting rhythms are organized in distinct zones in parameter space, leading to a global organization that should be applicable to the dynamics in a large class of excitable media.

DOI: 10.1103/PhysRevLett.94.028105 PACS numbers: 87.18.Hf, 05.45.–a, 82.40.Ck, 89.75.Da

Excitable media, such as the Belousov-Zhabotinsky reaction [1,2], aggregating slime mold [3], catalytic oxidation of CO on Pt [4], and cardiac tissue [5–11], display diverse spatiotemporal patterns. Understanding the factors that lead to particular types of organization of spatiotemporal patterns is of special importance in the cardiac context since abnormal types of organization are associated with dangerous or even fatal cardiac rhythms [5]. Dynamic behaviors observed in cardiac preparations include propagation from a pacemaker site, stable rotating spiral waves [6], unstable spiral waves that break up during propagation [7], and bursts of activity associated with the initiation and termination of spiral waves [8,9]. However, the way in which these different dynamical regimes arise as the parameters describing the cardiac medium vary is not known. In this Letter, we demonstrate transitions from periodic targets to spirals that spontaneously initiate and terminate, and to patterns with multiple fractionated wave fronts by changing culture conditions in experiments or by changing parameters in a theoretical model. Quantitative characterization of the spatiotemporal patterns [12] indicates that there may be self-organized behavior with dynamical patterns over a range of spatiotemporal scales.

To study the spatiotemporal patterns in excitable systems, we investigate a spatially heterogeneous cardiac cell monolayer preparation whose properties can be modified by changing the density of cells, and by adding a drug, α glycerrhetinic acid (αGA), that uncouples the intercellular connections. Figure 1 shows the dynamics of a monolayer of cardiac cells [13] plated at three different densities under different concentrations of αGA and imaged using a calcium-sensitive fluorescent dye. Each row in Fig. 1 represents data from one monolayer under increasing levels of gap junction blockade. Typical activation patterns for each of the nine culture conditions are represented as contour maps of activation times. Above each contour map, we plot the summed activity from the four center pixels over time. Bursting rhythms are defined as rhythms consisting of rapid activity of five or more activations with a period of ≤ 0.75 sec, followed by a period of quiescence ≥ 2.5 sec.

Depending on the experimental conditions, the monolayers display target waves generated at a constant rate, stable spiral waves, spiral waves that spontaneously start and stop, giving rise to a bursting rhythm, or irregular activity consisting of a mix of target patterns and self-terminating spiral waves. At high plating densities, monolayers predominantly display target patterns (5/6 cases) or stable spiral waves (1/6 cases) with no wave breaks. The

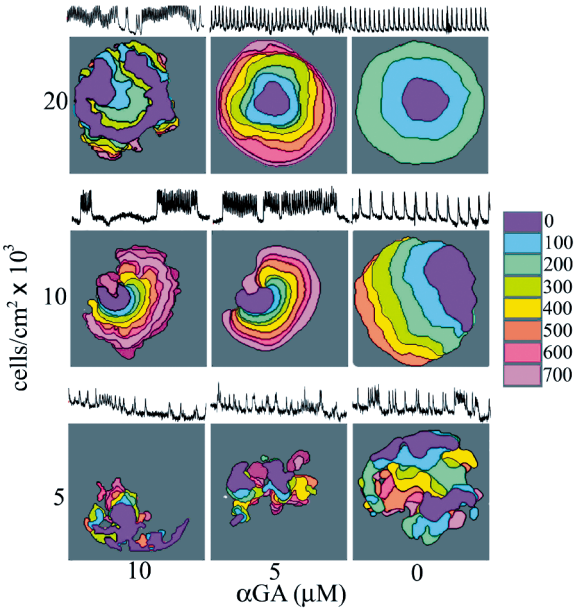

FIG. 1 (color). The activity of embryonic chick heart monolayers plated at three different densities under different concentrations of gap junction blocker αGA visualized with calcium-sensitive fluorescent dye. Each box is approximately 0.8 cm^2. A trace above each panel shows the activity for 50 sec of the four center pixels. The images are presented as activation plots which show the overlayed location of active cells at 100 msec intervals.

activity is periodic with a constant interbeat interval. For intermediate plating densities we observe target patterns (3/6 cases) and spiral waves (3/6 cases) with a small number of spiral centers. The dynamics are usually characterized by a constant interbeat interval, but can display a bursting rhythm (1/6 cases). Wave fronts appear to be smooth and display relatively few wave breaks. For low plating densities, waves are fractured and form multiple spirals (6/6 cases). Activation fronts may initiate as target patterns, but frequently break and form multiple spiral centers. Rhythms are aperiodic and often (4/6 cases) display bursting activity.

The addition of αGA converts periodic target patterns to bursting rhythms. The concentration of αGA needed to convert the rhythm depends on the density of the monolayer. The addition of 5 μM αGA to the high density preparation slows the wave velocity from 3.0 to 1.2 cm/sec but does not generate wave breaks. The addition of 10 μM αGA causes the dynamics to change from a regularly beating target pattern to spiral wave driven bursting. The addition of 5 μM αGA to monolayers plated at intermediate densities changes most target patterns to spiral wave driven bursting. The addition of 10 μM αGA introduces wave breaks but does not change the overall pattern of activity. The addition of αGA to the low density preparation acts to slow the wave velocity but does not change the pattern of activation.

Decreases of density and increases of αGA lead to similar effects, so that there are similar dynamics for preparations along the diagonal from the upper left hand corner to the lower right hand corner in Fig. 1. These data are consistent with the hypothesis that the local spatial organization of cells determines the global dynamics. Reducing cell coupling decreases the number of locally interacting cells by changing the size of the neighborhood, while reducing plating density lowers the number of cells within a neighborhood of a given size.

In order to isolate the important features that lead to the diverse spatiotemporal patterns, we use a cellular automation model of excitable media that has been modified from earlier formulations [8,14,15]. Simulations are carried out on a 100×100 square lattice. To introduce heterogeneity, we randomly locate each site in a square of unit length centered at its original unperturbed lattice site [16]. To model changes in the density of the preparation, we randomly remove cells leaving a fraction σ. Each site i at time (t) is assigned a state, $u_i(t)$. The state is an integer: 0 is a rest state; states $1, 2, \ldots, E$ are excited states; states $E + 1, E + 2, \ldots, E + R$ are refractory states; state $E + R + 1$ is identified with the rest state 0. The update rule for the state of a site is as follows: if $1 < u_i(t) < E + R$, then $u_i(t + 1) = u_i(t) + 1$. If $u_i(t) = 0$, then $u_i(t + 1) = 0$, unless it becomes excited so that $u_i(t + 1) = 1$ on the next time step. This can occur in two different ways:

Spread of excitation from neighboring cells.—This occurs if

$$\frac{\sum_{D[j,i]<r;\ 0<u_j(t)\leq E}}{\sum_{D[j,i]<r;u_j(t)=0 \text{ or } u_j(t)>E}} > \theta_i(t+1), \qquad (1)$$

where $D[j, i] = |x_j - x_i| + |y_j - y_i|$ is the distance between cell j and cell i; (x_j, y_j) is the location of cell j; $\theta_i(t + 1)$ is the excitation threshold for cell i at time $(t + 1)$ (see below); and the summation is over all cells within a distance r of cell i.

Random spontaneous activity.—For a cell in state $u_i(t) = 0$, we assume there is a probability ρ that $u_i(t + 1) = 1$.

Cardiac muscle is less excitable after rapid activity. This effect is often called fatigue [17]. We add a rate dependent fatigue term in order to model the slowing and termination of spiral wave activity observed in the experiments. The fatigue term of cell i at time $(t + 1)$ is $\gamma_i(t + 1) = \gamma_i(t) + F_{\text{add}}$ if $u_i(t + 1) = 1$, and $\gamma_i(t + 1) = \gamma_i(t) \times F_{\text{sub}}$ if $u_i(t + 1) \neq 1$. The fatigue term is added to a minimum threshold value θ_{min}, and the threshold is set to $\theta_i(t + 1) = \theta_{\text{min}} + \gamma_i(t + 1)$.

In this study, we investigate the effects of changing σ, r, and F_{sub}. The other parameters are set to $E = 6$, $R = 7$, $\rho = 0.001$, $F_{\text{add}} = 0.02$, and $\theta_{\text{min}} = 0.35$.

Figure 2 shows the dynamics for the model for different neighborhood sizes and density values. The model displays target patterns for high density values and large neighborhood sizes. Spirals do not form for these parameters because broken wave fronts seal at the initiation site and the wave does not develop wave breaks. The model displays reentrant dynamics for smaller neighborhood sizes and lower densities. Unidirectional block at the initiation site generates spiral waves. The spiral tip tends to increase its meander as fatigue accumulates. The spiral tip eventually collides with the boundary of the simulation grid, termi-

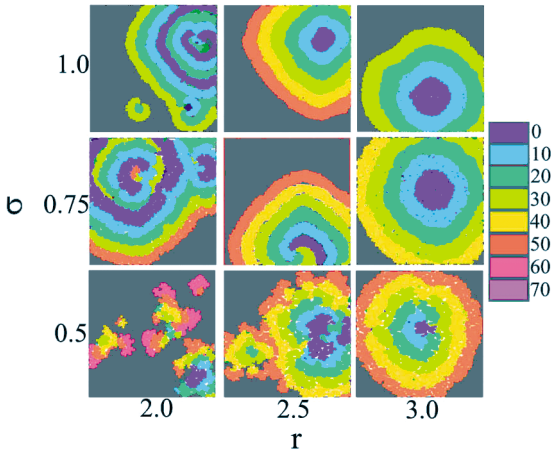

FIG. 2 (color). The dynamics of the model for different values of density and neighborhood size. The position of the wave front at different times is shown for the first propagated pulse. For this simulation $F_{\text{sub}} = 0.999$. The images are represented as activation plots showing the overlayed location of active cells at ten iterate intervals.

nating activity. This process repeats for some parameters, giving rise to a bursting rhythm.

We employ a coherent cluster analysis [12] to compare the spatiotemporal dynamics of the model data with the experimental results. Frames are stacked along the time axis to create a space-time cube. Neighboring active sites within the cube are joined to form space-time clusters. The spatiotemporal entropy is calculated from $S = -\sum_s v_s \ln v_s$ [12], where v_s is the normalized value of the total volume of all clusters for a given cluster size s [18]. The entropy values for the experimental results for different values of density and αGA are shown in Fig. 3(a). Entropy is low ($S < 1.0$) for dense, well coupled preparations that show target patterns or stably rotating spiral waves due to the presence of large cluster sizes. Entropy increases ($S > 1.0$) for preparations with multiple spiral waves. The entropy for the model is shown in Fig. 3(b). High entropy is found for parameters that give rise to fractionated wave fronts. The entropy values are comparable to the values obtained from the experimental results.

The properties of the cellular automation model are further assessed by analyzing three different geometries for different values of r and σ. Activity is classified by numerically determining the number of spiral tips and recording activation times of cells near position $(0, 0)$. The activity is classified as targets (no spiral tips, infrequent activation times), stable spirals (less than four spiral tips, frequent sequential activation times), or bursts (target patterns interspersed with spiral wave driven runs of rapid activity). Parameters that lead to bursting dynamics are shown in Fig. 3(c). The model displays target patterns for high values of r and σ, bursting spirals for intermediate values of r and σ, and wave breaks or block for low values of r and σ.

The cluster size distributions for parameters corresponding to two panels in the center column in Figs. 1 and 2 are shown in Fig. 4. The distributions are dominated by large clusters for parameters that give rise to target patterns in the experiment and model [Figs. 4(a) and 4(c)]. For parameters that give rise to fractured spiral waves with multiple cores [Figs. 4(b) and 4(d)], the distributions display a linear scaling region for small cluster sizes in the log-log plot. Although definite conclusions cannot be made because of the comparatively small size of the tissue culture and the noise that is inherent in the data, the linear scaling in the log-log plot suggests that for some ranges of parameters there is scaling behavior similar to the scaling observed by Jung and colleagues in astrocyte cultures [12].

The experimental and numerical studies lead us to suggest a scheme for the global organization for spatiotemporal dynamics for heterogeneous excitable media in which there is fatigue. In proposing this scheme we assume that in the zone in which the medium is strongly excitable (corresponding here to the dense preparation without αGA) target waves propagate as concentric circles from a point source, and spiral waves circulate stably. Bursting dynamics are observed for parameters in the shaded region in Fig. 5. For low values of fatigue ($F_{\text{sub}} < 0.994$), the model does not display bursts but generates stable spirals or target patterns depending on the value of r. For intermediate and high values of fatigue, bursts are observed for certain values of r. For low r, bursting dynamics are observed only for high values of F_{sub}. Bursting dynamics are observed for progressively lower values of F_{sub} as r increases from 1.5 to 2.5. For $r > 2.5$, bursts are not observed.

The dynamics observed in this Letter assume that excitability is independent of cell density and that spiral waves are stable in the absence of heterogeneity. If these conditions are not met, different dynamics can be observed as parameters are varied. Panfilov [11] found that reduced connectivity stabilizes spiral waves in models which display spiral wave breakup at high connectivity. Lee *et al.* [3] found that low plating densities favor target waves over spiral waves in slime mold cultures because broken wave fronts do not form spiral waves at low densities due to decreased excitability.

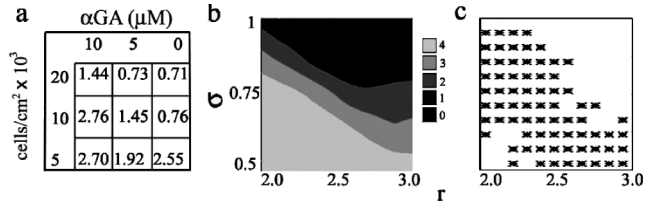

FIG. 3. The dynamics of the experimental preparation and the model for different values of density and cell-cell coupling. (a) Entropy values calculated for 500 consecutive frames for the experimental data shown in Fig. 1. (b) Entropy values calculated for parameters of the model, shown as a contour plot. Since the size of large clusters is constrained by the boundary of the simulation, we consider clusters of greater than 10 000 pixels to be in the same size class in order to minimize boundary effects. (c) Model parameters that give rise to bursting dynamics are indicated with black crosses. The results for the model were obtained by simulating three different geometries at each parameter point.

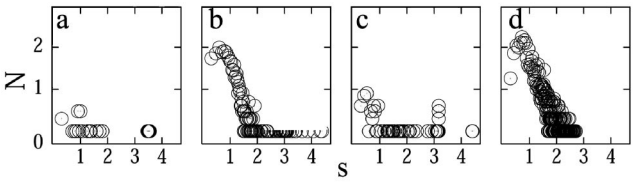

FIG. 4. Cluster size distributions for 500 frames from the experimental data under intermediate gap junction block (αGA = 5 μM) for different densities (panels a and b) and 6000 iterates of the model (panels c and d) for $r = 2.5$ for different density values. (a) Cluster size distribution for a high density (20×10^3 cells/cm^2) monolayer. (b) Cluster size distribution for a low density (5×10^3 cells/cm^2) monolayer. (c) Cluster size distribution for the model for high density $\sigma = 1$. (d) Cluster size distribution for the model for low density $\sigma = 0.5$. Cluster sizes for the model were divided by a scaling factor of 3 to fit the data.

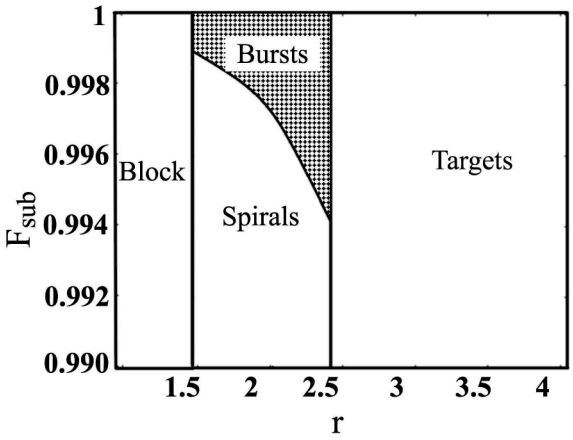

FIG. 5. Schematic global organization in the cellular automaton based on computations at 2000 values evenly spaced on the F_{sub}, r parameter space. Each parameter point was tested for three randomly generated arrays.

This work gives insight into previous observations in diverse systems. Chemical reactions where negative feedback is experimentally imposed [2,4] display spatiotemporal patterns similar to the bursting spirals we observe in our preparation as a consequence of changes of density or the addition of αGA. Moreover, the diseased heart in which coupling and/or excitability is reduced as a consequence of growth of fibrous tissue [19] or medication [20] is susceptible to the spontaneous initiation of dangerous arrhythmias that may be associated with spiral wave activity. Although these arrhythmias may be sustained, they often spontaneously terminate, leading to behaviors that are similar to the bursting dynamics observed here [21].

Although deterministic partial differential equations representing excitable media display bifurcations in dynamics as parameters are changed, in stochastic heterogeneous excitable media of finite size, the characterization of different dynamical regimes is not as developed. The current study provides further evidence that in some regions of parameter space there are spatiotemporal structures over a broad range of scales. The global organization of dynamics described here should be observed in a variety of different excitable systems.

This research has been supported by funding for the Canadian Heart and Stroke Foundation, CIHR, MITACS, and the NIH National Center for Research Resources. We would like to thank Dr. P. Jung for helpful discussions.

[1] A. T. Winfree, *When Time Breaks Down: The Three-Dimensional Dynamics of Electrochemical Waves and Cardiac Arrhythmias* (Princeton University Press, Princeton, NJ, 1987); J. Maselko and K. Showalter, Physica (Amsterdam) **49D**, 21 (1991); K. Agladze *et al.*, Science **264**, 1746 (1994); R. Imbihl and G. Ertl, Chem. Rev. **95**, 697 (1995); M. Bar *et al.*, J. Phys. Chem. **100**, 19 106 (1996); I. Sendina-Nadal *et al.*, Phys. Rev. E **58**, 1183 (1998); I. Schebesch and H. Engel, Phys. Rev. E **57**, 3905 (1998); S. Clar *et al.*, Physica (Amsterdam) **266A**, 153 (1999); F. Xie *et al.*, Phys. Rev. E **63**, 031905 (2001).

[2] V. K. Vanag *et al.*, Nature (London) **406**, 389 (2000).

[3] K. J. Lee, E. C. Cox, and R. E. Goldstein, Phys. Rev. Lett. **76**, 1174 (1996).

[4] M. Bertram *et al.*, Phys. Rev. E **67**, 036208 (2003).

[5] J. Jalife *et al.*, Nature (London) **392**, 78 (1998).

[6] E. Entcheva *et al.*, J. Cardiovasc. Electrophysiol. **11**, 665 (2000); N. Bursac *et al.*, Circ. Res. **91**, 45 (2002).

[7] A. Arutunyan *et al.*, Am. J. Physiol. Heart. Circ. Physiol. **280**, H1905 (2001).

[8] G. Bub *et al.*, Proc. Natl. Acad. Sci. U.S.A. **95**, 10 283 (1998).

[9] S. Hwang, K. Yea, and K. J. Lee, Phys. Rev. Lett. **92**, 198103 (2004).

[10] A. Karma, Phys. Rev. Lett. **71**, 1103 (1993); F. H. Fenton *et al.*, Chaos **12**, 852 (2002).

[11] A. V. Panfilov, Phys. Rev. Lett. **88**, 118101 (2002).

[12] P. Jung *et al.*, J. Neurophysiol. **79**, 1098 (1998); P. Jung *et al.*, Phys. Rev. E **61**, 2095 (2000).

[13] Cardiac monolayers are prepared as described previously [8,14]. Briefly, chick embryonic ventricular heart cells are plated at varying densities (5 to 20×10^3 cells/cm^2). After 72 h, the preparations are loaded with Calcium Green (5 μM, 30 min), and calcium fluorescence is monitored at 20 frames per second with a cooled charge-coupled device mounted to a macroscope.

[14] G. Bub, A. Shrier, and L. Glass, Phys. Rev. Lett. **88**, 058101 (2002); G. Bub *et al.*, J. Cardiovasc. Electrophysiol. **14**, s229 (2003).

[15] J. M. Greenberg and S. P. Hastings, Bull. Am. Math. Soc. **6**, 84 (1978); M. Gerhardt, H. Schuster, and J. J. Tyson, Science **247**, 1563 (1990).

[16] M. Markus and B. Hess, Nature (London) **347**, 56 (1990).

[17] A. Noma and N. Tsubio, J. Physiol. **382**, 193 (1987); J. Billette, R. Meteyer, and M. St. Vincent, Circ. Res. **62**, 790 (1988); A. M. Kunysz, A. Shrier, and L. Glass, Am. J. Physiol. **273**, C331 (1997).

[18] Clusters are formed by joining adjacent excited sites in the (x, y, t) grid, where each site has six adjacent sites. In order to facilitate comparison, the same algorithm was used to group clusters in the data from the experiment and model. The activation wave front in the data was found by taking the first derivative of the calcium fluorescence, and adjusting the threshold value so that wave fronts overlap in adjacent frames. The widths of wave fronts in the model are adjusted to the minimum that allows overlap between wave fronts in adjacent frames. Since the duration of cardiac action potentials is known to be greater than 50 msec, clusters with duration $\leq$50 msec in the experiment and duration $\leq$4 iterates in the model were removed from the analysis.

[19] J. M. de Bakker *et al.*, Circulation **88**, 915 (1993).

[20] D. S. Echt *et al.*, N. Eng. J. Med. **324**, 781 (1991).

[21] J. Parkinson and C. Papp, Br. Heart J. **9**, 241 (1947).